APPLICATION OF THE RADIAL DISTRIBUTION FUNCTIONS FOR QUANTITATIVE ANALYSIS OF NEUROPIL MICROSTRUCTURE IN STRATUM RADIATUM OF CA1 REGION IN HIPPOCAMPUS

Yuriy Mishchenko

Author:
Yuriy Mishchenko
Izmir University of Economics, Izmir, Turkey

Address:
Izmir University of Economics, Sakarya Sok No: 156, 35330, Izmir, Turkey
Email:
yuriy.mishchenko@gmail.com,
phone: 90(530)2446240

ABSTRACT

Various structures in the brain contain important clues to the brain's development and function. Among these, the microscopic organization of neural tissue is of particular interest since such organization directly affects the formation of local synaptic connectivity between axons and dendrites, serving as a potential factor in the brain's development. While the organization of the brain at large and intermediate lengths had been well studied, the organization of neural tissue at scales of micrometers remains largely unknown. In particular, at present it is not known what specific structures exist in neuropil at those scales, what effect such structures have on the formation of synaptic connectivity in the brain, and what processes shape the small-scale organization of neuropil. In this work, we present an analysis of recent 3D electron microscopy reconstructions of blocks of tissue of hippocampal CA1 neuropil from rat s. radiatum to offer new insights into these questions. We propose a new statistical method for systematical analysis of the small-scale organization of neuropil, based on an adaptation of the approach of radial distribution functions from statistical physics. Our results show that the micrometer-scale organization of hippocampal CA1 neuropil can be well understood as a disordered arrangement of axonal and dendritic processes without significant small-scale coordination. We observe several deviations from this picture in the distributions of glia and dendritic spines, and discuss their significance. Finally, we shed some light on the relationship between the small-scale organization of neuropil and local synaptic connectivity.

KEYWORDS: neuropil organization, neuroanatomy, electron microscopy reconstruction, neurodegeneration, radial distribution function

1 Introduction

Understanding the brain's anatomical structure is an important goal of neuroscience both from the point of view of producing new insights into the principles of brain's organization (Arbib et al., 1997; de Bono et al., 2005; Hatton, 1990; Sporns et al., 2004, 2005) as well as better understanding of the brain's development and disorders (Brambilla et al., 2003; Castellanos et al., 2002; Garrard et al., 1998; Geschwind, 1975; Good et al., 2002; Uhlhaas and Singer, 2006). Diverse anatomical structures are readily visible in the brain at variety of scales. At the largest scales, the organization of the brain into specific regions and functional areas had been well established (Brodmann and Garey, 2005; Damasio, 2005; Kandel et al., 2000). At intermediate scales, structures such as cortical layers (Kandel et al., 2000; Nolte, 2002), cortical columns (Freeman, 2003), topographic mappings (Adams and Horton, 2003; Montero et al., 1977), ocular dominance patterns (Erwin et al., 1995; Miller et al., 1989) and orientation selectivity patterns in visual cortex (Bosking et al., 1997; Ohki et al., 2005), as well as topographic mappings in auditory (Morosan et al., 2001; Pickles, 2012) and somatosensory cortex (Nelson, 2001) are also known. A range of genetic, biomolecular, and neural activity mechanisms are known to be associated with the formation and development of these structures, providing clues about how the brain develops and functions (Dickson, 2002; Ferster and Miller, 2000; Keil et al., 2010; McLaughlin and O'Leary, 2005; Parrish et al., 2007; Tear, 1999; Wolf et al., 2011; Wong, 1999).

Despite this extensive body of knowledge, the anatomical organization of the brain at the smallest, micrometer scales – at the level of neuropil – remains essentially unknown today. Nonetheless, such organization is of general as well as of practical interest in neuroscience. It had been hypothesized that the small-scale organization of neuropil immediately affects the formation of synaptic connectivity between axons and dendrites, via the availability of local axonal and dendritic partners for new synaptic connections (Braitenberg and Schuz, 1998; Peters, 1979; Stepanyants and Chklovskii, 2005; Stepanyants et al., 2008). Abnormal changes in the small-scale structure of neural tissue, therefore, can contribute to neurodegenerative disorders, frequently connected to the degeneration of synaptic connectivity in neural tissues (Bonda et al., 2010; Hamos et al., 1989; Raff et al., 2002; Scheff et al., 2006; Terry, 2000).

In the present study, we attempt to shed new light onto the micrometer-scale organization of neuropil using recent anatomical serial section Transmission Electron Microscopy (ssTEM) reconstructions of blocks of neural tissue

from stratum radiatum of hippocampal CA1 in rat (Mishchenko, 2009; Mishchenko et al., 2010). To address the above questions, we propose a new quantitative approach based on an adaptation of the statistical tool of radial distribution function from material sciences (Chandler, 1987; McQuarrie, 2000; Sandler, 2010). Radial distribution function is a statistical tool that can be used to characterize spatial correlations between different structural elements in a material. Radial distribution functions have been used extensively in material science to describe the micro-scale organization of various materials including alloys, solutions, and colloids.

We conduct a direct measurements of radial distribution functions for hippocampal CA1 neuropil using the neuropil reconstruction data available from (Mishchenko et al., 2010). We analyze obtained distributions using statistical and modeling approaches. The result of this analysis indicates that the organization of neuropil at micrometer scales most closely resembles a disordered arrangement of filament-like neural processes, spherical spines, and irregular glia fragments. We discuss the deviations from this picture observed in the distribution of spines and glia. Finally, we analyze the variations in the spine density of dendritic segments in relation to the structure of their surrounding neuropil, as quantified by the radial distribution function, and show the absence of significant correlations between local neuropil of a dendrite and that dendrite's density of spines, rejecting the notion of strong influence of surrounding neuropil on dendrites' spine formation.

To summarize, in this work we present new results related to the study of organization of brian neural tissue at the scales of 1-10 micrometers. We analyze examples of several blocks of rat neuropil tissue from hippocampal CA1 region, reconstructed in detail in 3D using ssTEM. We apply a new quantitative approach to the analysis of the organization of such tissue blocks, based on an adaptation of radial distribution functions from material science, and systematically quantify the presence of any "non-random" arrangements in neuropil organization at micrometer lengths. Our findings show that the organization of neuropil at micrometer scales is disordered and stochastic, to the extent characterized by the radial distribution functions we measured.

2 Materials and Methods

2.1 Experimental data

Three approximately cubic blocks of hippocampal neuropil tissue had been reconstructed using ssTEM in (Mishchenko et al., 2010) and used here to perform the analyses of this work.

Specificallty, the datasets 1, 3, and 4 from in (Mishchenko et al., 2010) were used; the dataset 2 was not used because of its small size, a 30 μm^3 neuropil block surrounding a single dendritic spine. All volumes were from the middle of s. radiatum about 150 to 200 micrometers from the hippocampal CA1 pyramidal cell layer. Volumes 1 and 3 were from a perfusion-fixed male rat of the Long-Evans strain weighing 310 gm (postnatal day 77), as described in (Harris and Stevens, 1989)), and volume 4 was from a hippocampal slice from a postnatal day 21 male rat of the Long-Evans strain fixed, as described in (Fiala et al., 2003). All animal procedures were performed in accordance with relevant regulatory standards, as described in (Fiala et al., 2003; Harris and Stevens, 1989).

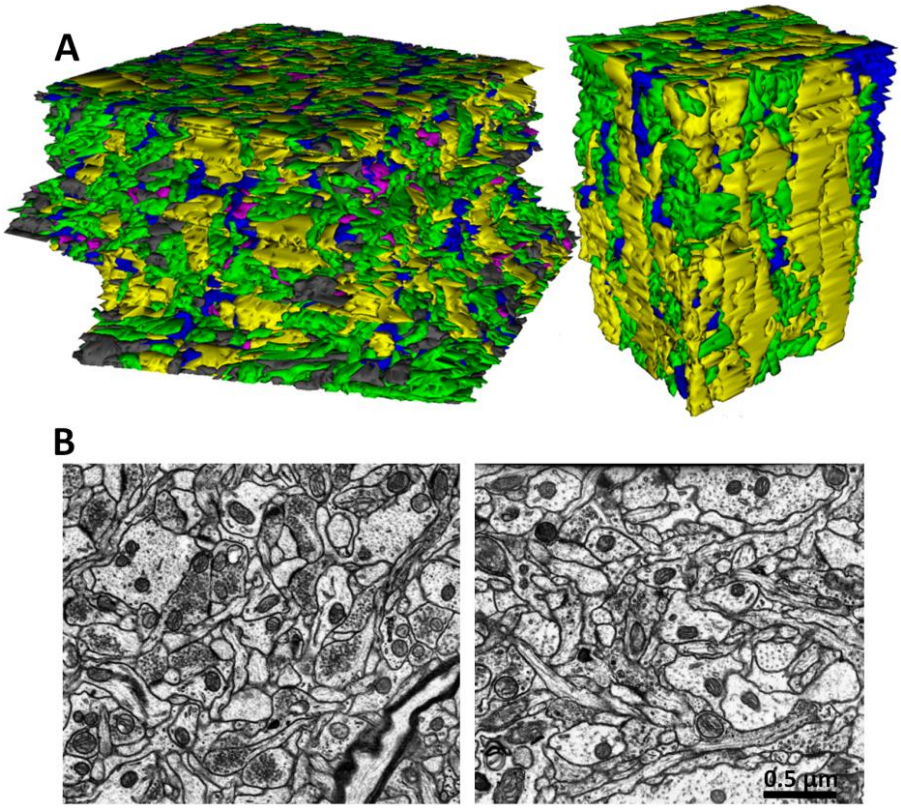

Figure 1 Dense ssTEM reconstructions of neural tissue volumes reveal complex micro-organization of neural tissue. (A) An example of dense 3D ssTEM reconstruction "Volume 1" from (Mishchenko et al., 2010) (left) and "Volume 4" from (Mishchenko, 2009) (right). These neuropil blocks measure 9.1 × 9.0 × 4.1 μm^3 and 6.0 × 4.3 × 5.1 μm^3. Different colors identify neural processes of different types: green for axons, yellow for dendrites, magenta for spines, and blue for glia fragments. Gray are the objects that could not be classified based on the ssTEM images alone. (B) An example of ssTEM micrograph images from "Volume 1" (left) and "Volume 4" (right), used in digital reconstructions of 3D volumes in (A).

Briefly, the series of ultrathin sections were cut at ~45-50 nm using an ultramicrotome, mounted and counter stained with saturated ethanolic uranyl acetate followed by Reynolds lead citrate. The sections were then photographed on JEOL 1200EX and 1230 electron microscope (JEOL, Peabody, MA) at magnification of 10,000X or 5,000X, and stored as series of digital images at 4.4 nm/pixel. The neuropil in these images was reconstructed digitally using the approach of (Mishchenko, 2009) and stored as 3D volumes of labeled data for further analysis. The reconstructions totaled 670 μm^3 and contained 1900 fragments of different neural processes (Figure 1).

2.2 Radial distribution functions

Radial distribution functions are introduced in material science as the measure of the density of structures (atoms or molecules in material science) of a certain sort in concentric radial shells surrounding another typical "reference" structure (again atom or a molecule in material science applications) in material (Figure 2A). Radial distribution functions characterize the spatial correlations present in a material and, in that capacity, provide a powerful tool for systematic quantification of the small-scale organization of materials and systems with complex organization. In material science, radial distribution functions have been commonly used to analyze the organization of materials such as alloys, solutions, colloids, etc.

Radial distribution functions can be visualized easily by counting the number of particles present in each concentric spherical shell, surrounding a fixed reference particle. If particles in a system are distributed completely randomly and uniformly, then such count will grow in direct proportionality to the volume of the concentric shells, whereas their density in each shell will remain constant. That is, the radial distribution functions in the situation that the relative positions of the element of a material are completely random are simply constant. If a system possessed interactions between particles, leading to such particles having different likelihoods of appearing at different relative distances from each other, so then the above density also will vary from shell to shell, producing a radial distribution function that peaks at certain distances and may have other distinctive features. In general, therefore, we can say that in disordered materials the radial distribution functions are featureless and flat, and in ordered materials the radial distribution functions have peaks and other distinctive features representative of the spatial correlations existing in those systems.

For example, Figure 2B shows several radial distribution functions calculated for different idealized arrangements of neuronal processes in neuropil. Panel B1

shows such an example of an arrangement that is perfectly ordered, that is, where all neuronal processes are oriented in the same direction and are also spatially well aligned. The radial distribution function for this case is shown in the right subpanel: such respective radial distribution shows strong peaks representative of the strong spatial correlations in this arrangement. Panel B2 shows an example arrangement where neural processes are partially disordered, that is, where their positions are less well coordinated and also their directions may vary somewhat. In this arrangement, the radial distribution function still shows peak-like features, but such features become weaker and less pronounced, due to the destruction of the correlations in the structure. Finally, panel B3 shows an example of such an arrangement that is completely disordered, that is, where the headings of neural processes are completely random as are their positions. The radial distribution function in this case is flat and shows no significant features.

As had been discussed above, the conventional definition of radial distribution functions relies on using concentric spherical shells, in order to quantify the changes in elements' density with the distance from a reference point-like particle. In the case of neuropil tissue, however, we cannot adopt this convention and develop a slightly different approach, because axonal and dendritic processes in neuropil have long, elongated fiber-like shapes and also their cross-section shapes are highly irregular, at micrometer length scales. Specifically, for neuropil we define the radial distribution functions as the average density of different neural processes, namely *axons*, *dendrites*, *spines*, and *glia*, in concentric *cylindrical* shells around the surface of a reference neuronal process, Figure 2C. The radial distribution functions defined and calculated specifically for neuropil will be also referred to in this work as the neuropil's structure functions.

As a final note of this section, it should be emphasized that radial distribution functions are a strong signature of a particular type of organization of neural tissue, but not every type. In particular, radial distribution functions are sensitive to positional coordination between neural processes, that is, the situations such that the presence of one neural process influences the likelihoods of finding other neural processes around it. However, radial distribution function will not be sensitive to structure aspects such that do not manifest in spatial positions of neural processes, or that depend on non-spatial properties of neuronal processes such as being projections of excitatory/inhibitory neurons, etc. Such latter structure aspects are not the targets of the present paper.

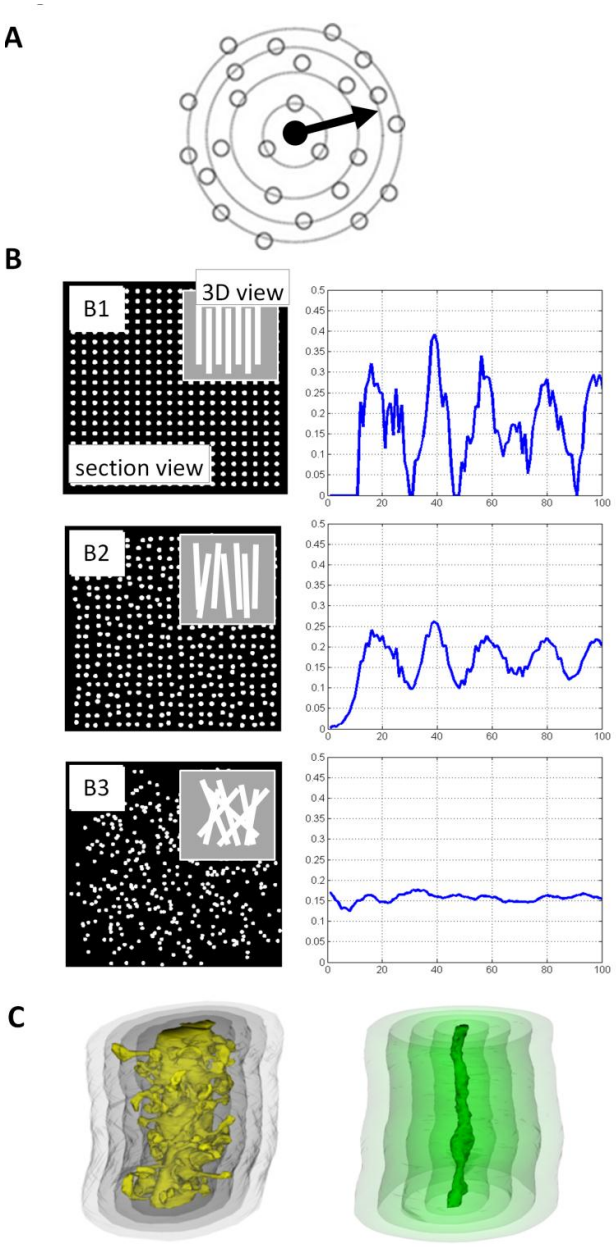

Figure 2 Radial distribution functions as characteristics of small-scale structure of neuropil. (A) Radial distribution functions offer a powerful tool for characterization of the small-scale structure of complex materials and arrangements. Radial distribution functions are calculated as the change in density of particles of certain sort in concentric shells surrounding a "typical" reference particle. Radial distribution functions can be visualized as counts of particles of each sort in every concentric shell around a fixed reference particle, further divided by the volume of each shell. (B) An illustration of radial distribution functions calculated for model neuronal process arrangements. Panel B1 shows an arrangement that is perfectly ordered, that is, such where all neuronal processes are oriented in the same direction and are also spatially aligned (left). The radial distribution function calculated for this arrangement shows strong peaks representative of the spatial correlations existing in the arrangement (right). Panel B2 shows an arrangement where neuronal processes are partially disordered (left). In this arrangement, the radial distribution function still possesses peaks and other features, but these are less pronounced, due to the destruction of correlations in the arrangement (right). Panel B3 shows an arrangement that is completely disordered (left). The radial distribution function in this case is flat and lacks any features with statistical significance (right). Note that this figure is an illustration, whose purpose is to exemplify the three main regimes of radial distribution functions. This illustration should not be used as a detailed comparison for the real radial distribution functions calculated for rat hippocampal neuropil below. (C) In neural tissue, the shapes of neuronal processes, presenting the objects of interest, are fiber-like and highly irregular in cross-section. For this reason, we modify the conventional "spherical" definition of radial distribution functions to use cylindrical concentric shells instead, constructed away from the surface of axonal or dendritic processes in neuropil. The calculation of such radial distribution function is illustrated in this figure using a series of concentric cylindrical shells at different distances away from the surface of one reference dendrite (left) or axon (right). Radial distribution functions for neuropil then are defined as the average density of neuronal processes of different type (that is, axons, dendrites, spines or glia) within such shells, for different distances away from the reference axon or dendrite's surface.

2.3 Measurement of radial distribution functions in experimental data

In order to calculate the radial distribution functions in the experimental data for hippocampal neuropil, we first constructed a series of equidistant concentric cylindrical shells from the surface of each axon and dendrite in experimental datasets (approximately 1500 neural processes in total). This was done by calculating numerically the Euclidian distance transform (EDT) of each neuronal process in the dataset. Distance transform is an operation that assigns to every point in a volume the shortest distance from that point to the surface of a reference object, here, a neuronal process. This calculation was performed using a custom implementation of EDT algorithm for very-large-size datasets in Matlab described in (Mishchenko, 2015). The set of equidistant surfaces of such distance transforms constituted a set of concentric cylindrical shells which was used for calculating the radial distribution functions in the experimental neural tissue data above, such as illustrated in Figure 2C.

Once concentric cylindrical shells had been constructed for all neuronal processes in the dataset, the radial distribution functions for each neuronal process were calculated by computing the volume density of neuropil structures of different type contained in each concentric shell of each neuronal process, at the step of 13.2 nm for Volume 1 and Volume 3 and 8 nm for Volume 4. The latter difference was due to the different pixel size of the digitized Volume 4 (that is, 8 nm/pixel vs. 4.4nm/pixel).

Thus produced radial distribution functions for each neuronal process were averaged over all reference axons and dendrites, in order to produce class-average axon- and dendrite-specific radial distribution functions for neuropil volumes.

In the case of dendrites, the above procedure was carried out after first truncating all dendritic spines at the bases of their necks, using an algorithm, in order for the concentric shells to describe the real distances from the dendritic shafts and not other elements of dendritic processes (such as spines or spine necks). All dendritic shafts obtained first algorithmically were also examined manually, in order to insure that no spines remained attached, which would have damaging results on the measurements of the radial distribution functions.

2.4 Measurement of the size distribution of axonal and dendritic cross-sections

In order to measure the distribution of the local sizes of axonal and dendritic cross-sections in neuropil, we first evaluated

3D distance transform inwards of each neural process in the dataset. This had the effect of assigning to each point inside neural processes the shortest distance from that point to the surface of the containing process, outwards. The centerline of each neural process then was calculated as the set of points where such inward distance transform had a local maximum along at least two out of three orthogonal directions. The values of that distances transform were then collected along centerlines inside each neuronal process. Such quantities characterized the distribution of the smaller diameters of roughly eliptical cross-sections of irregularly shaped neuronal processes in neuropil, sampled uniformly along the length of such processes at the step of approximately 50 nm (that is, the EM section thickness). The class-specific distributions for each neuropil volume were then calculated by taking an average of each size distribution over all axonal and dendritic processes.

2.5 Local neuropil random mixing model

In order to quantitatively describe the most salient features observed in measured neuropil's radial distribution functions, here we propose a relatively simple mathematical model of neuropil's local random mixing. The aim of this model is to describe how the radial distribution functions for reference axonal and dendritic processes change with the distance from the surface of reference process. The model primarily takes into account mathematically the changes in the density of different neuropil components within concentric cylindrical shells because of the termination and re-emergence of axonal and dendritic cross-sections in such shells as they sweep through the neuropil volume away from the reference object.

Thus, if we imagine ourselves moving together with concentric cylindrical shells away from the surface of a reference axon or dendrite, it is easy to imagine that the cross-sections of other axons and dendrites would emerge, grow, contract, and disappear within such shells as they cross over different axonal and dendritic processes in nearby neuropil. The volume occupied by such axonal and dendritic cross-sections in each shell will change, as the result of these processes of emergence and disappearance of nearby profiles of axonal and dendritic processes.

In random mixing model, we account for these processes as additions and removals of the volume associated with each type of neuropil component occurring at constant rates. If we imagine a large cylindrical surface moving through a volume of uniformly mixed axonal and dendritic processes, then such rates with which axonal and dendritic cross-sections appear and disappear in it are defined by the inverse of their respective diameters.

In other words, a cylindrical shell that sweeps through neuropil has axons appear and disappear in it more frequently, due to their smaller radii, while dendritic cross-sections will appear and remain in the shell for much longer periods of time, because they are larger. Thus, the volume associated with axons in concentric cylindrical shells moving away from reference neuronal processes is added and removed at high rate, while that associated with dendrites is added and removed at slower rate.

To formalize the above picture mathematically and to obtain its results for neuropil's radial distribution functions, we consider the process of moving over a set of concentric cylindrical shells away from the surface of one reference axon or dendrite. If the average diameters of axonal and dendritic processes in the volume are given by d_{axn} and d_{dnd}, respectively, then the probability of an axon or a dendrite cross-section disappearing in the cylindrical shell as we move over a distance Δx can be approximately described as $\Delta x/d_{axn}$ and $\Delta x/d_{dnd}$. The space vacated in the shell due to such terminations should be re-partitioned among newly emerging axons and dendrites, which clearly has to occur in the proportion of the total surface areas of axonal and dendritic processes in the volume, $n_{axn}\pi d_{axn}L$: $n_{\ dnd}\pi d_{dnd}L$. Here, L is a constant defining the linear size of the sample volume and n_{axn}, n_{dnd} are the number densities of axons and dendrites in the volume, respectively. Then, clearly, πdL is the surface area of one neural process viewed as a straight cylinder of diameter d and length L, and the above is the ratio of the total surface areas of such axonal and dendritic processes per unit volume.

We denote the relative densities of axonal and dendritic processes in cylindrical shells at distance x away from the surface of reference axon or dendrite as $N_{axn}(x)$ and $N_{dnd}(x)$, respectively. Then, the processes qualitatively discussed above mathematically can be modeled by two equations for the evolution of $N_{axn}(x)$ and $N_{dnd}(x)$ along x;

$$\Delta N_{axn}(x) = -N_{axn}(x)\frac{\Delta x}{d_{axn}} + \frac{n_{axn}d_{axn}}{n_{axn}d_{axn} + n_{dnd}d_{dnd}}\left(N_{axn}(x)\frac{\Delta x}{d_{axn}} + N_{dnd}(x)\frac{\Delta x}{d_{dnd}}\right)$$

$$\Delta N_{dnd}(x) = -N_{dnd}(x)\frac{\Delta x}{d_{dnd}} + \frac{n_{dnd}d_{dnd}}{n_{axn}d_{axn} + n_{dnd}d_{dnd}}\left(N_{axn}(x)\frac{\Delta x}{d_{axn}} + N_{dnd}(x)\frac{\Delta x}{d_{dnd}}\right)$$

These equations describe the change in the volumes occupied in concentric cylindridcal shells by axonal and dendritic processes, occurring over a step away of size Δx. The first term represents the termination of axons and dendrites with frequencies $\Delta x/d_{axn}$ and $\Delta x/d_{dnd}$, respectively, and the second term represents the re-partitioning of the vacated space among newly emerging axons and dendrites in the ratio of their surface areas, $n_{axn}d_{axn} : n_{\ dnd}d_{dnd}$. Also note that $N(x)$ are relative densities, that is, $N_{axn}(x) + N_{dnd}(x) = 1$ for all x.

The above equations are a linear system of finite-difference equations that can be solved using standard methods. The solution yields several notable predictions for the behavior of neuropil's radial distribution functions. Specifically, at small distances, $x \approx 0$, we find that the radial distribution functions should have the ratio equal to that of the total surface areas of dendritic and axonal processes in the entire dataset, $N_{axn}(x \approx 0) : N_{dnd}(x \approx 0) \approx n_{axn}d_{axn} : n_{dnd}d_{dnd}$ (this can be seen by taking $N_{axn}(0) = 1$ or $N_{dnd}(x) = 1$ and performing a single step Δx in the above equations). At large distances, $x \to \infty$, the values of the radial distribution functions are defined by the ratio of the average volume densities of axonal and dendritic processes in the entire dataset, $N_{axn}(\infty) : N_{dnd}(\infty) \approx n_{axn}{d_{axn}}^2 : n_{dnd}{d_{dnd}}^2$ (this can be seen by enforcing in the above equations the condition $\Delta N_{axn}(\infty) = \Delta N_{dnd}(\infty) = 0$ and inspecting consequences). Given $d_{dnd} > d_{axn}$, it follows then that these ratios differ by the factor of d_{dnd}/d_{axn}. Referring to Table 3 in (Mishchenko et al., 2010), one obtains $d_{dnd}/d_{axn} \approx 3$, so that it is predicted that the ratio of neuropil's radial distribution functions for axons and dendrites will change by a factor of 3 as one moves from small to large distances away from a reference neuronal process. The transition between the small distance and the large distance occurs in the model radial distributions exponentially on the scale $l \approx d_{dnd}\frac{1+S_{dnd}/S_{axn}}{1+V_{dnd}/V_{axn}}$, where $S_{dnd}/S_{axn}$and V_{dnd}/V_{axn} are the ratios of dendritic and axonal surface and volume fractions in the sample, respectively. Referring to Figure 2 in (Mishchenko et al., 2010), we obtain $l \approx 0.5$ micrometer. Therefore, it is expected that neuropil's radial distribution functions will completely relax within the distance of about 0.5 micrometers from the surface of reference object. Finally, the radial distribution functions are found in random mixing model to be the same, whether the reference object is an axon or a dendrite. That is, the dendrite- and axon-specific radial distribution functions in neuropil are predicted to be the same. Going a bit ahead of ourselves we note that all of these predictions are confirmed in the measured radial distribution functions.

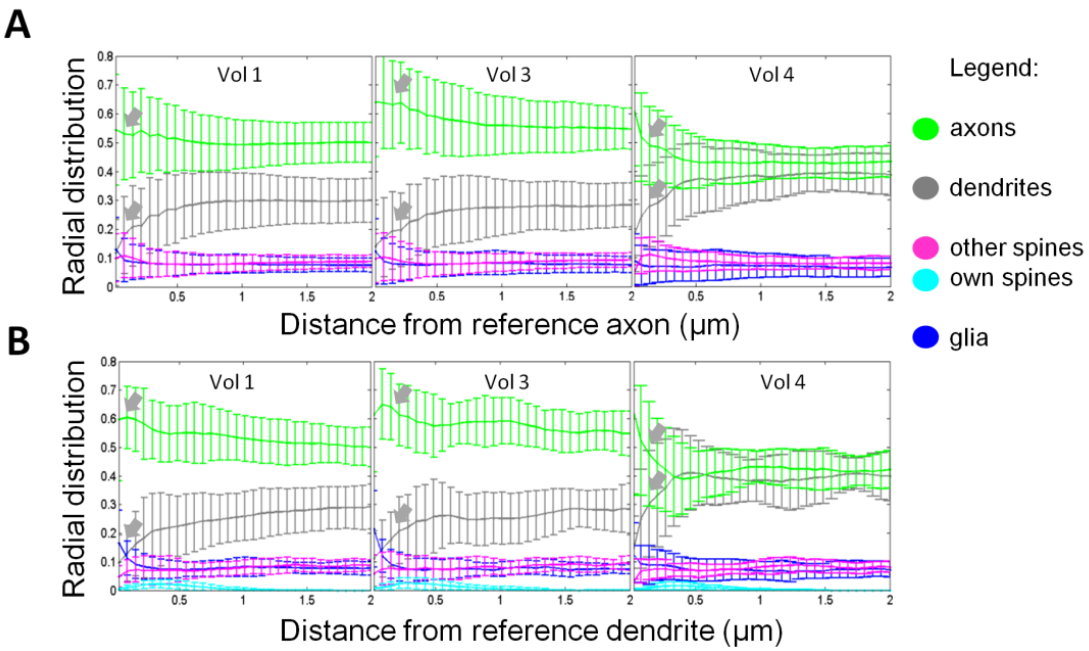

Figure 3 The radial distribution functions of hippocampal CA1 neuropil. (A) Radial distribution functions measured for different neuropil components relative to axonal reference processes in sample neuropil volumes 1, 3 and 4. (B) Radial distribution functions measured for different neuropil components relative to dendritic reference processes in sample neuropil volumes 1, 3 and 4. The measured radial distribution functions show predominantly flat behavior, indicating lack of significant spatial correlations among neuropil components at the scales of 0.5 to several micrometers. The error bars represent the variation in the radial distribution functions around different axonal and dendritic references in the samples.

3 Results

3.1 Organization of hippocampal CA1 neuropil at micrometer scales

Reconstruction of complete volumes of neuropil tissue had been recently produced using electron microscopy. A quick inspection of these reconstructions, Figure 1, reveals complex small-scale organization of hippocampal neuropil without apparent patterns. However, one cannot immediately conclude whether this lack of features is due to the absence of any structures in neuropil at micrometer scales or because such structures are complex and are visually non-apparent.

In order to provide an answer to this question, we perform a measurement of radial distribution functions in real hippocampal neuropil, making use of the reconstructions of blocks of rat s. radiatum hippocampal CA1 tissue from (Mishchenko et al., 2010). Please refer to Materials and Methods for the discussion of the definition and the properties of such radial distribution functions. We will also refer to such radial distribution functions specifically in neuropil as the neuropil's *structure functions*. Figure 3 shows the result of these measurements.

The main feature of the measured neuropil structure functions in Figure 3 is their flat behavior at the distances above of approximately 0.5 micrometers. A linear regression performed on these structure functions in the range of 0.5-2 micrometers gives the coefficient of regression $R=0.019\pm0.030$ micrometer^{-1} and the residual mean-square-error (MSE) $MSE=0.0043\pm0.0022$ micrometer^{-1} for dendritic structure functions, and $R=-0.014\pm0.032$ micrometer^{-1} and $MSE=0.0035\pm0.0015$ micrometer^{-1} for axonal structure functions. Therefore, either dendritic or axonal structure functions are flat in the region of distances away from reference neuronal process above 0.5 micrometers. This behavior of the structure functions should be interpreted as the absence of correlations in the relative position of neuronal processes in neuropil at distances above 0.5 micrometers.

The measured structure functions in Figure 3 show rise/drop-features at the distances below 0.5 micrometers, which should be interpreted as the presence of correlations among the neural processes in neuropil at these smaller distances (gray arrows in Figure 3).

The short-range rise/drop features can be explained as the effect of physical contact interactions between adjacent neural processes in densely packed neuropil. That is, if at large distances away from a reference process the neural processes can mix uniformly, near the surface of that process the presence of the process's boundary causes adjacent neural processes to re-align along it, and induces correlations in the positions of such processes reflected by the above small-distance features.

This effect can be described not just qualitatively, as above, but quantitatively using the model of local random mixing of neuropil (Materials and Methods), which reproduces all the main properties of the observed neuropil structure functions. In particular, this model predicts that near the surface of the reference object the ratio of the axonal and dendritic structure functions should equal the ratio of the total axonal and dendritic surface areas in neuropil volume. This ratio can be calculated from overall neuropil statistics such as listed in (Mishchenko et al., 2010), and equals 6:1 for volumes 1 and 3 and 3:1 for volume 4. This is in excellent agreement with the measured neuropil structure functions in Figure 3. Local random mixing model further predicts that at large distances the ratio of axonal and dendritic structure functions will drop to that of the overall axonal and dendritic volume densities, which can be calculated again from neuropil's bulk data given (Mishchenko et al., 2010) as 2:1 for volumes 1 and 3 and 1:1 for volume 4. Again, this is in excellent agreement with Figure 3. The transition between the two values is

predicted to occur exponentially on the length scale of $l \approx 0.5$ micrometers, primarily determined by the average dendritic and axonal diameters. This is again in excellent agreement with Figure 3. Finally, the structure functions are predicted to have the same behavior around axonal and dendritic reference processes, and again this is in excellent agreement with the measurements.

Certain differences can be noted between the structure functions measured in volumes 1 and 3 and that in volume 4. These differences can be attributed to volume 4 being slice preparation and volumes 1 and 3 being perfusion fixed, or to that volume 4 is from a young (P21) and volume 1 and 3 are from a mature (P77) rat. Inspection of a greater number of reconstructed tissue volumes is needed to answer this question. Unfortunately, no other similar reconstructions are available at this time.

In summary, the experimental neuropil radial distributions that we measure are very well described by the local mixing model of neuropil, presented in Materials and Methods. Therefore, we arrive at the conclusion that the organization of hippocampal CA1 neuropil at the micrometer scales, as quantified by the neuropil structure functions, can be very well described by a random mixing of axonal and dendritic processes without significant local order.

3.2 Orientational organization of neuronal processes in hippocampal CA1 neuropil

Even though the micrometer-scale organization of neural processes in neuropil does not exhibit spatial ordering, it can still exhibit a global order in terms of directional alignment. In fact, it is well known from existing anatomical studies that axonal and dendritic processes in hippocampus are running in approximately perpendicular directions (Amaral and Witter, 1989; Cajal, 1909; Schaeffer, 1892; Westrum and Blackstad, 1962). Here, we measure the distribution of such headings of dendritic and axonal processes in our samples on micrometer scale. We find that the approximately perpendicular organization of dendrites and axons is observed even at these tiny scales, Figure 4. We observe that dendrites tend to run collinearly approximately in one direction, orthogonal to the CA1 cell-body layer, and axons tend to pass mostly within the plane of cell-body layer.

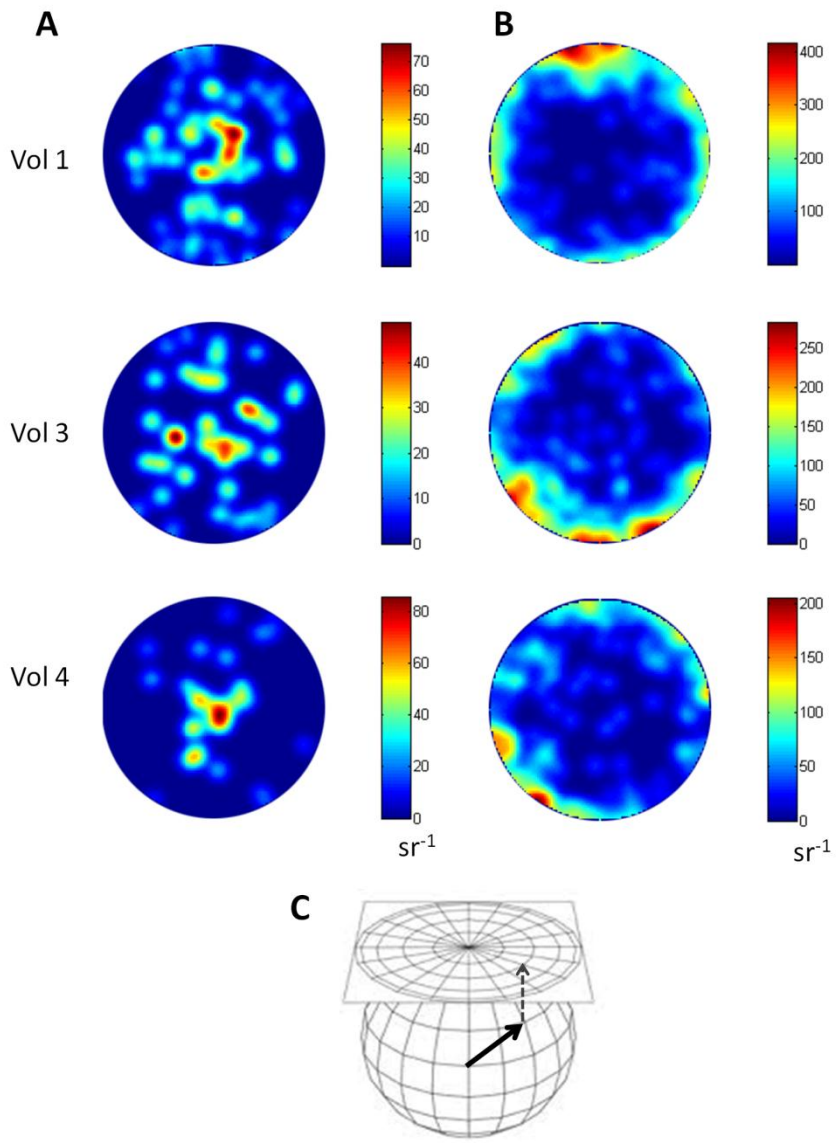

Figure 4 The local directional organization of hippocampal CA1 neuropil. (A-B) The distribution of the headings of dendritic (A) and axonal (B) processes in the samples, shown as azimuthal projection. All projections are centered on the average heading direction of the dendritic processes in each sample. Measured local directional organization of hippocampal CA1 neuropil reveals approximately perpendicular headings of dendrites and axons. The dendrites are found to run mostly collinearly in the direction perpendicular to the plain of the CA1 cell-body layer. The axons are found to run predominantly within that plane. Additionally, the axonal distribution is found to exhibit two distinct directional components: a collinear component and a diffuse component, each containing approximately 50% of all axons. (C) The azimuthal projection plots here show how the counts of dendrites and axons moving in given direction in each sample volume is represented on the projection plot. Each direction of one dendritic or axonal process can be thought of as vector pointing on a unit sphere. Such vector then gets projected onto the unit sphere's equatorial plane, making up the projection plots shown here in (A) and (B). Different colors represent the count of neuritis whose directions were projected to the same point, per unit of the unit-sphere's area.

The axonal directional distribution is also observed to possess an interesting two-component structure, with approximately half of all axons traveling in a single collinear bundle and the rest appearing to traverse the sample diffusely, in all directions within the plane parallel to the cell-body layer. The division of axons in these two components is 50/50% and is very interesting. However, we were unable to identify any significant correlates of this division with other axonal properties accessible from EM data (for example, axonal diameter). A more detailed study in the future may help shed light onto this peculiar feature of microscopic axonal organization in CA1 neuropil.

3.3 Organization of glia and dendritic spikes in hippocampal CA1 neuropil

The random mixing model prescribes that the radial distributions of neuropil components around a reference neural process should not depend on the type of that process, either a dendrite or an axon. This condition, in particular, is met rather well for the measured structure functions of axonal and dendritic neuropil components. For the distribution of dendritic spines (spine-heads) and glia, however, we observe deviations from that rule. In particular, the distribution of dendritic spines is revealed by the respective structure functions to be significantly higher at the proximity of axonal rather than dendritic processes, and for glia we observe the reverse affinity towards dendritic as opposed to axonal surfaces, Figure 5A-B.

In the case of glia, more specifically, the average relative density near dendritic processes is measured as 0.17 ± 0.01, while that near axonal surfaces is 0.13 ± 0.005 (Figure 5B). Therefore, we observe the difference in the relative density of glia near dendritic and axonal processes at p-value <0.001. One can note that spines in neuropil commonly protrude away from dendrites and towards axons, in order to touch the latter and establish synaptic contacts. Thus, the difference observed in the distribution of dendritic spines, Figure 5A, may be deemed natural. Similarly, the differences observed in the distribution of glia fragments indicates the presence of factors affecting the distribution of glia in neuropil favoring dendrites against axons.

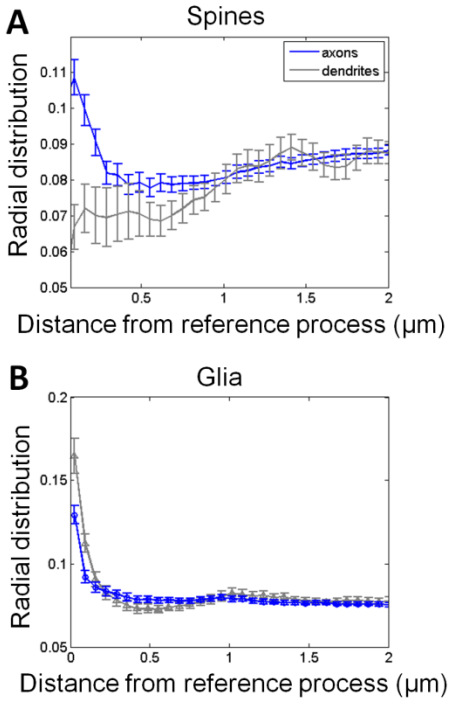

Figure 5 The distributions of glia fragments and dendritic spines in hippocampal CA1 neuropil. (A) The radial distribution functions of dendritic spines relative to axonal and dendritic reference processes. (B) The radial distribution functions of glia relative to axonal and dendritic reference processes. The legend is for all plots. Error bars are the standard error of the mean. Radial distribution functions of dendritic spines and glia reveal deviations from random mixing model of neuropil. Specifically, the radial distribution functions of dendritic spines reveal significantly higher affinity towards axonal as opposed dendritic surfaces, and that of glia reveals a reverse affinity towards dendritic as opposed to axonal surfaces. While for dendritic spines the observed affinity can be natural, given dendritic spines protruding away from dendrites and towards axons to form synapses, for glia the observed effect implies presence of novel mechanisms realizing preferential attraction of glia towards dendrites.

3.4 Local distributions of neuronal process sizes in hippocampal CA1 neuropil

The distribution of sizes of neural processes in neuropil has been a subject of significant attention in neuroanatomy (Braitenberg and Schuz, 1998; Mishchenko et al., 2010; Shepherd and Harris, 1998; Sorra and Harris, 2000). A comprehensive measurement of average neural processes' sizes had been performed in (Mishchenko et al., 2010). Here, we extend these measurements to characterize the distribution of local neural processes' sizes, that is, such measured along neural processes' lengths, rather than on average for each one neuronal process. The sizes of axonal and dendritic processes are known to vary significantly even within a single process over the space of just a few micrometers (Braitenberg and Schuz, 1998). Therefore, such local size measure is important for understanding how the neuropil is organized on small scales.

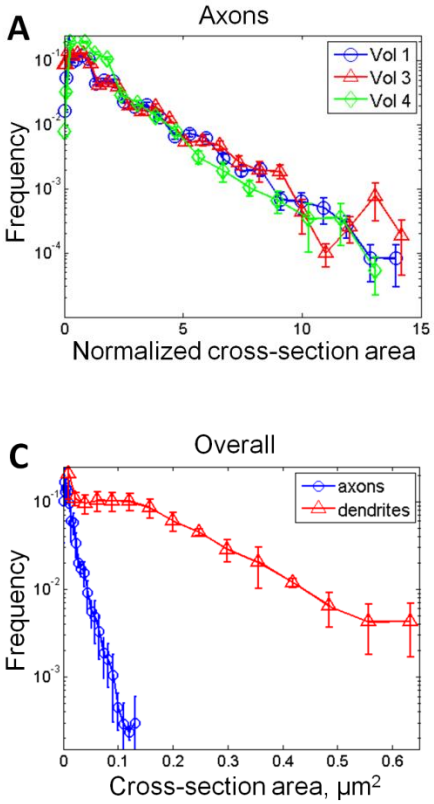

Figure 6 The distribution of axonal and dendritic local cross-section sizes. (A) The distribution of local sizes of axonal cross-sections in sample volumes 1, 3 and 4, normalized to the average axonal cross-section in each volume. The legend shown is for A and B. The error bars are the standard error of the mean. (B) The distribution of local sizes of dendritic cross-sections in sample volumes 1, 3 and 4, normalized to the average dendritic cross-section in each volume. All distributions are well described by the same exponential maximal entropy distribution, suggesting a common mechanism of their origin. (C) The overall distributions of axonal and dendritic cross-section sizes shown on absolute scale; the slope of the distributions is clearly different due to the different size of average axonal (approximately 0.2 micrometers) and dendritic (approximately 0.66 micrometers) cross-section diameters.

We present our measured size distributions in Figure 6. We observe that these distributions are essentially exponential, both for axonal and dendritic neuropil components. For spine-heads, the exponential shape of size distribution had been known in the past, and an explanation had been proposed based on information-theoretic arguments affecting synapses' information capacity (Varshney et al., 2006). Here, we observe that the same shape is characteristic of the local size distributions for all neuropil components, so that a more generic explanation may be appropriate. We find that an explanation based on the properties of exponential distributions as the maximum entropy distributions (Jaynes, 2003) can particularly naturally explain these observations. In maximum entropy interpretation, the observed size distributions can be explained as the outcome of stochastic exchanges of small amounts of space in space-filling neuropil packing in the context of competition for limited space between axonal and dendritic neuronal processes (Chklovskii et al., 2002).

3.5 The relationship between small-scale neuropil organization and local synaptic connectivity

It had been hypothesized in the past that the small-scale organization of neuropil has significant effect on the formation of synaptic connections, by affecting the availability of local axonal and dendritic partners for synaptic connections (Braitenberg and Schuz, 1998; Peters, 1979; Stepanyants and Chklovskii, 2005; Stepanyants et al., 2008). Changes in such organization, therefore, may be deemed to contribute or be responsible for the disruptions of synaptic connectivity in neural tissues, such as observed in many neurodegenerative disorders (Bonda et al., 2010; Hamos et al., 1989; Raff et al., 2002; Scheff et al., 2006; Terry, 2000).

In order to examine this relationship in our study, we examine the variations of spine densities of different dendritic segments in the dataset in relation to the structure and composition of the neuropil immediately surrounding them, as quantified by the radial distribution or structure functions. We group all dendritic segments into three categories of high, medium, and low spine-densities, and compare the structure functions for dendritic references from each such group. Our results are presented in Figure7. We observe that the spine-density graded-structure functions exhibit no significant variations with respect to the reference dendrite's spine density, indicating lack of relation between dendrites' spine density and local neuropil surroundings, Figure 7B-D. Some variations do appear to emerge in Figure 7B-D; however, at current level these are below one standard deviation and, therefore, cannot be claimed as statistically significant at this point.

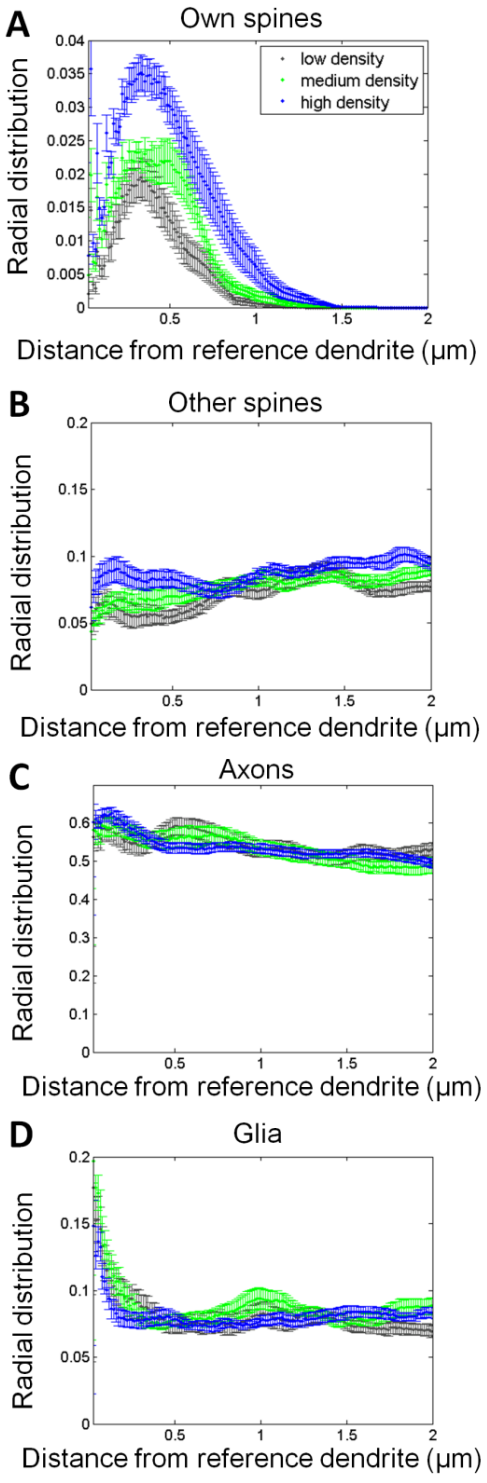

Figure 7 The variations in neuropil organization around dendrites with different spine density. (A) The radial distributions of reference dendrites' own spines reveal higher utilization of surrounding neuropil by higher spine-density dendrites. Also, these radial distributions indicate that the dendrites with all densities of spines tend to place their spines stereotypically at the same distance away from dendritic shaft, in a zone 0 to 1 micrometer away from the shaft with the maximum spine density achieved at distances of 400 nm away from the dendrite's surface. (B-D) The other radial distribution functions exhibit no significant differences in the surrounding neuropil in relation to the reference dendrite's spine-density. Shown are (B) the radial distributions of the spines of other dendrites, (C) the radial distributions of axons, and (D) the radial distributions of glia, graded by the spine density of the reference dendrite. The low spine-density group is defined as the lowest 50% of spine density dendrites, next 25% comprise the medium spine-density group, and the highest 25% comprise the high-density group. The legend shown is for all graphs. The error bars are the standard error of the mean.

A significant difference is observed in the distribution of the reference dendrites' own spines, Figure 7A. In this case, the dendrites with higher spine density are clearly observed to exhibit higher densities of own spines in immediately adjacent neuropil. This may appear as a tautological consequence of trifurcating dendrites into low, medium, and high densities; however, it is not merely so. Since the dendrites with higher density of spines should place a larger number of spines into their neuropil surrounding, the above result indeed is not unexpected. However, although higher spine density does mean more spines, such spines could be of smaller size leading to about similar utilization of nearby neuropil by the spines in dendrites of all spine-density groups. Alternatively, "excess" spines for spinier dendrites could be placed further out from the dendritic shaft, resulting in uniform but more "extended" radial distributions of own spines for spinier dendrites. Instead, we observe that in all spine-density groups the structure function has the same shape, but different absolute scaling. This should be interpreted that spines are created by dendrites essentially in a "fixed" manner – with similar size and at similar distance away from the dendritic shaft, just spinier dendrites make more of such "standard" spines.

Finally, interestingly in Figure 7B we observe that the structure function of the spines of other dendrites around reference dendrites for all spine-densities stay flat, the coefficient of linear regression $R=0.0090$ micrometer^{-1} with $MSE=0.0031$ micrometer^{-1}. We can interpret this indicator as the indifference of spines of other dendrites to the presence of the spines of reference dendrite. In other words, Figure 7B demonstrates that the spine zones of nearby dendrites in neuropil are free to interpenetrate and overlap without any difficulties, or mutual alteration of nearby dendrites' spines.

4 Discussion

While the ubiquity of anatomical structure in the brain at macro and mesoscales is well known, the structural organization of the brain at the smallest, micrometer scales remains largely unknown. In this work, we aim to fill this gap by examining the structural organization of several blocks of neural tissue from s. radiatum of hippocampal area CA1 in rat, recently digitally reconstructed from serial section electron microscopy data.

Dense reconstructions of neuropil in (Mishchenko, 2009; Mishchenko and Paninski, 2012; Rivera-Alba et al., 2011) offer unique insight into neuropil's small-scale organization in the sense that they not only provide the reconstructions of a large number of dendritic and axonal processes at nanometer resolution, but

also place these in the context of their immediate surroundings. To gain insights into the micrometer-scale organization of neuropil in this work, we calculate the radial distribution functions for the samples of neuropil in s. radiatum hippocampal area CA1 reconstructed in other study in the above manner. We analyze obtained structure measurements statistically and by using a modeling approach. We show that the micrometer-scale organization of neuropil is essentially consistent with disordered packing of fiber-like axonal and dendritic processes in a tight, space-filling arrangement. At very small distances below 0.5 micrometer, correlations among neural processes are observed and attributed to the effects of physical contact of neural processes, seen as relatively solid shapes in the settings of dense neuropil packing. We also present the measurement of local orientation anisotropy of neural tissue in hippocampal neuropil, as well as the local size distribution of neural processes in the same tissue.

We observe deviations in the micrometer-scale distributions of dendritic spines and glia, whereas dendritic spines are observed to be preferentially located near axonal processes and glia is observed with higher densities near dendritic processes. While for dendritic spines such affinity can be expected, given that spines protrude away from dendrites in order to contact axons and create synapses, there are no known established mechanisms that could explain the observed excess of glia near dendrites. The observations here indicate the presence of yet unknown neurobiological factors affecting the development of glia and its affinity to dendrites in neuropil.

Finally, we examine the question of the interaction between the small-scale organization of neuropil and local synaptic connectivity. While it may be expected that local organization of neuropil affects the formation of small-scale synaptic connectivity in significant ways, we do not observed that to be the case. Instead, we observe that the synaptic densities of dendritic segments appear to vary completely independently of the structure and composition of neuropil surrounding such segments.

Our analysis relies on characterization of neuropil's organization using radial distribution functions. While these provide a systematic way for assessing the small-scale organization of neuropil, it should be taken into account that structure functions are but one of the possible measures of structure. Specifically, this measure is sensitive to positional coordination, that is, the situation where the presence of one neural process affects the likelihood of finding another neural process of specific type in the vicinity. Respectively, our results are about the lack of any spatial

coordinations in neuropil on micrometer scales, but cannot be taken to widely, for example, to imply the absence of other types of structure such as related to neuritis being excitatory/inhibitory type, etc.

It should be also noted that our findings had been produced using a limited sample of hippocampal CA1 neuropil and, therefore, may not apply in other circumstances. Given the past neuroanatomical literature indicates a substantial level of similarity in neural tissues across different cortex regions (Braitenberg and Schuz, 1998), we do believe that these observations are indicative of the larger picture of neuropil's organization in mammalian cerebral cortex.

Our study focused on a specific question of the structural organization of neuropil viewed as a system of primarily axons and dendrites. Without doubt this focus leaved a large number of interesting questions beyond the scope of the paper. A particularly interesting one other question is the structural organization of neuropil around synapses and spines, especially in relation to the types of synapses and other their features. Another set of interesting questions is related to technically similar comparison of the differences between healthy and abnormal neural tissues. Such topics without doubt will present an interesting venue for future extensions of this work.

Acknowledgements

The author acknowledges the financial support from Bilim Akademisi – The Science Academy, Turkey, under BAGEP program and the support from the BAP fund – the Fund for Scientific Research Projects, of Toros University, Mersin, Turkey.

References

Adams, D.L., and Horton, J.C. (2003). A Precise Retinotopic Map of Primate Striate Cortex Generated from the Representation of Angioscotomas. J. Neurosci. *23*, 3771–3789.

Amaral, D.G., and Witter, M.P. (1989). The three-dimensional organization of the hippocampal formation: a review of anatomical data. Neuroscience *31*, 571–591.

Arbib, M.A., Erdi, P., and Szentagothai, J. (1997). Neural Organization: Structure, Function, and Dynamics (A Bradford Book).

Bonda, D.J., Bajić, V.P., Spremo-Potparevic, B., Casadesus, G., Zhu, X., Smith, M.A., and Lee, H.-G. (2010). Review: Cell cycle aberrations and neurodegeneration. Neuropathol. Appl. Neurobiol. *36*, 157–163.

de Bono, M., Villu Maricq, A., Bono, M., Villu Maricq, A., de Bono, M., V., M.A., and Villu Maricq, A. (2005). Neuronal substrates of complex behaviors in C.

elegans. Annu. Rev. Neurosci. *28*, 451–501.

Bosking, W.H.W.W.H.W., Zhang, Y., Schofield, B., and Fitzpatrick, D. (1997). Orientation Selectivity and the Arrangement of Horizontal Connections in Tree Shrew Striate Cortex. J. Neurosci. *17*, 2112.

Braitenberg, V., and Schuz, A. (1998). Cortex: statistics and geometry of neuronal connectivity. (Berlin: Springer).

Brambilla, P., Hardan, A., di Nemi, S.U., Perez, J., Soares, J.C., and Barale, F. (2003). Brain anatomy and development in autism: Review of structural MRI studies. Brain Res. Bull. *61*, 557–569.

Brodmann, K., and Garey, L.J. (2005). Brodmann's: Localisation in the Cerebral Cortex (Springer).

Cajal, R. (1909). Histologie du systeme nerveux de l'homme et des vertebres (Paris: Madrid, Instituto Ramon y Cajal).

Castellanos, F.X., Lee, P.P., Sharp, W., Jeffries, N.O., Greenstein, D.K., Clasen, L.S., Blumenthal, J.D., James, R.S., Ebens, C.L., Walter, J.M., et al. (2002). Developmental Trajectories of Brain Volume Abnormalities in Children and Adolescents With Attention-Deficit/Hyperactivity Disorder. J. Am. Med. Assoc. *288*, 1740–1748.

Chandler, D. (1987). Introduction to Modern Statistical Mechanics (New York: Oxford University Press).

Chklovskii, D.B.D.B.D.B.D.B.D.B., Schikorski, T., and Stevens, C.F. (2002). Wiring optimization in cortical circuits. Neuron *34*, 341–347.

Damasio, H. (2005). Human Brain Anatomy in Computerized Images (Oxford university press).

Dickson, B.J. (2002). Molecular mechanisms of axon guidance. Science (80-.). *298*, 1959–1964.

Erwin, E., Obermayer, K., and Schulten, K. (1995). Models of Orientation and Ocular Dominance Columns in the Visual Cortex: A Critical Comparison. Neural Comput. *7*, 425–468.

Ferster, D., and Miller, K.D. (2000). Neural Mechanisms of Orientation Selectivity in the Visual Cortex. Annu. Rev. Neurosci. *23*, 441–471.

Fiala, J.C., Kirov, S.A., Feinberq, M.D., Petrak, L.J., George, P., Goddard, C.A., and Harris, K.M. (2003). Timing of neuronal and glial ultrastructure disruption during brain slice preparation and recovery in vitro. J. Comput. Neurol. *465*, 90–103.

Freeman, R.D.D. (2003). Cortical columns: a multi-parameter examination. Cereb. Cortex *13*, 70.

Garrard, P., Patterson, K., Watson, P.C., and Hodges, J.R. (1998). Category specific semantic loss in dementia of Alzheimer's type. Functional-anatomical

correlations from cross-sectional analyses. Brain *121*, 633–646.

Geschwind, N. (1975). The Apraxias: Neural Mechanisms of Disorders of Learned Movement. Am. Sci. *63*, 188–195.

Good, C.D., Scahill, R.I., Fox, N.C., Ashburner, J., Friston, K.J., Chan, D., Crum, W.R., Rossor, M.N., and Frackowiak, R.S.J. (2002). Automatic Differentiation of Anatomical Patterns in the Human Brain: Validation with Studies of Degenerative Dementias. Neuroimage *17*, 29–46.

Hamos, J.E., DeGennaro, L.J., and Drachman, D.A. (1989). Synaptic loss in Alzheimer's disease and other dementias. Neurology *39*, 355.

Harris, K.M., and Stevens, J.K. (1989). Dendritic spines of CA1 pyramidal cells in the rat hippocampus: serial electron microscopy with reference to their biophysical characteristics. J. Neurosci. *9*, 2982–2997.

Hatton, G.I. (1990). Emerging concepts of structure-function dynamics in adult brain: the hypothalamo-neurohypophysial system. Prog. Neurobiol. *34*, 437–504.

Jaynes, E.T. (2003). Probability Theory: The Logic of Science. (New York: Cambridge University Press).

Kandel, E., Schwartz, J., and Jessell, T. (2000). Principles of Neural Science (McGraw-Hill Medical).

Keil, W., Schmidt, K.F., Löwel, S., and Kaschube, M. (2010). Reorganization of columnar architecture in the growing visual cortex. Proc. Natl. Acad. Sci. *107*, 12293.

McLaughlin, T., and O'Leary, D.M. (2005). Molecular gradients and development of retinotopic maps. Annu. Rev. Neurosci. *28*, 327–355.

McQuarrie, D.A. (2000). Statistical Mechanics (University Science Books).

Miller, K.D., Keller, J.B., and Stryker, M.P. (1989). Ocular dominance column development: analysis and simulation. Science (80-.). *245*, 605–615.

Mishchenko, Y. (2009). Automation of 3D reconstruction of neural tissue from large volume of conventional serial section transmission electron micrographs. J. Neurosci. Methods *176*, 276–289.

Mishchenko, Y. (2015). A function for fast computation of large discrete Euclidean distance transforms in three or more dimensions in Matlab. Signal, Image Video Process. *9*, 19.

Mishchenko, Y., and Paninski, L. (2012). Efficient methods for sampling spike trains in networks of coupled neurons. Ann. Appl. Stat. *5*, 1893–1919.

Mishchenko, Y., Hu, T., Spacek, J., Mendenhall, J., Harris, K.M., and Chklovskii, D.B. (2010). Ultrastructural analysis of hippocampal neuropil from

the connectomics perspective. Neuron *67*, 1009–1020.

Montero, V.M., Guillery, R.W., and Woolsey, C.N. (1977). Retinotopic organization within the thalamic reticular nucleus demonstrated by a double label autoradiographic technique. Brain Res. *138*, 407–421.

Morosan, P., Rademacher, J., Schleicher, A., Amunts, K., Schormann, T., and Zilles, K. (2001). Human primary auditory cortex: cytoarchitectonic subdivisions and mapping into a spatial reference system. Neuroimage *13*, 684–701.

Nelson, R.J. (2001). The Somatosensory System: Deciphering the Brain's Own Body Image (CRC Press).

Nolte, J. (2002). The Human Brain: An Introduction to Its Functional Anatomy (Mosby).

Ohki, K., Chung, S., Chung, Y.H., Kara, P., and Reid, R.C. (2005). Functional imaging with cellular resolution reveals precise micro-architecture in visual cortex. Neuron *433*, 597–603.

Parrish, J.Z., Emoto, K., Kim, M.D., and Jan, Y.N. (2007). Mechanisms that regulate establishment, maintenance, and remodeling of dendritic fields. Annu. Rev. Neurosci. *30*, 399–423.

Peters, A. (1979). Thalamic input to the cerebral cortex. Trends Neurosci. *2*, 183.

Pickles, J.O. (2012). An Introduction to the Physiology of Hearing (Academic Press).

Raff, M.C., Whitmore, A. V., and Finn, J.T. (2002). Axonal Self-Destruction and Neurodegeneration. Science (80-.). *296*, 868–871.

Rivera-Alba, M., Vitaladevuni, S.N., Mishchenko, Y., Mischenko, Y., Lu, Z., Takemura, S.-Y., Scheffer, L., Meinertzhagen, I. a, Chklovskii, D.B., and de Polavieja, G.G. (2011). Wiring economy and volume exclusion determine neuronal placement in the Drosophila brain. Curr. Biol. *21*, 2000–2005.

Sandler, S.I. (2010). An Introduction to Applied Statistical Thermodynamics (John Wiley & Sons).

Schaeffer, K. (1892). Beitrag zur Histologie der Ammonshornformation. Arch Mikrosc Anat *39*, 611–632.

Scheff, S.W., Price, D.A., Schmitt, F.A., and Mufson, E.J. (2006). Hippocampal synaptic loss in early Alzheimer's disease and mild cognitive impairment. Neurobiol. Aging *27*, 1372–1384.

Shepherd, G.M., and Harris, K.M. (1998). Three-dimensional structure and composition of CA3->CA1 axons in rat hippocampal slices: implications for presynaptic connectivity and compartmentalization. J. Neurosci. *18*, 8300–8310.

Sorra, K.E., and Harris, K.M. (2000). Overview on the structure, composition, function, development, and plasticity of hippocampal dendritic spines. Hippocampus *10*, 501–511.

Sporns, O., Chialvo, D.R., Kaiser, M., and Hilgetag, C.C. (2004). Organization, development and function of complex brain networks. Trends Cogn. Sci. *8*, 418–426.

Sporns, O., Tononi, G., Kötter, R., Kotter, R., Kötter, R., and Kotter, R. (2005). The human connectome: a structural description of the human brain. PLoS Comput. Biol. *1*, e42.

Stepanyants, A., and Chklovskii, D.B. (2005). Neurogeometry and potential synaptic connectivity. TRENDS Neurosci. *28*, 387.

Stepanyants, A., Hirsch, J.A., Martinez, L.M., Kisvarday, Z.F., Ferecsko, A.S., and Chklovskii, D.B. (2008). Local Potential Connectivity in Cat Primary Visual Cortex. Cereb. Cortex *18*, 13–28.

Tear, G. (1999). Neuronal guidance: a genetic perspective. Trends Neurosci. *15*, 113–118.

Terry, R.D. (2000). Cell Death or Synaptic Loss in Alzheimer Disease. J. Neuropathol. Exp. Neurol. *59*, 1118–1119.

Uhlhaas, P.J., and Singer, W. (2006). Neural Synchrony in Brain Disorders: Relevance for Cognitive Dysfunctions and Pathophysiology. Neuron *52*, 155–168.

Varshney, L.R., Sjöström, P.J., and Chklovskii, D.B. (2006). Optimal information storage in noisy synapses under resource constraints. Neuron *52*, 409–423.

Westrum, L.E., and Blackstad, T.W. (1962). An electron microscopic study of the stratum radiatum of the rat hippocampus (regio superior, CA1) with particular emphasis on synaptology. J. Comput. Neurol. *119*, 281–309.

Wolf, L., Goldberg, C., Manor, N., Sharan, R., and Ruppin, E. (2011). Gene expression in the rodent brain is associated with its regional connectivity. PLoS Comput. Biol. *7*, e1002040.

Wong, R.O.L. (1999). Retinal waves and visual system development. Annu. Rev. Neurosci. *22*, 29–47.